JGR Space Physics

RESEARCH ARTICLE
10.1029/2021JA029651

Prompt Penetration and Substorm Effects Over Jicamarca During the September 2017 Geomagnetic Storm

B. G. Fejer[1], L. A. Navarro[2], S. Sazykin[3,†], A. Newheart[3], M. A. Milla[4], and P. Condor[4]

[1]Center for Atmospheric and Space Sciences, Utah State University, Logan, UT, USA, [2]Department of Electrical and Computer Engineering, University of Illinois Urbana-Champaign, Urbana, IL, USA, [3]Department of Physics and Astronomy, Rice University, Houston, TX, USA, [4]Jicamarca Radio Observatory, Instituto Geofisico del Peru, Lima, Peru

†Deceased 04 May 2021.

Key Points:

- Very strong changes on the vertical drifts and equatorial spread F intensity after dusk on September 7, 2017
- Very large eastward and westward electric field perturbations from about 19 to 22 LT, likely enhanced by substorms
- Strong short-lived response of equatorial spread F to a very large westward disturbance electric field at 19 LT

Correspondence to:

B. G. Fejer,
bela.fejer@usu.edu

Citation:

Fejer, B. G., Navarro, L. A., Sazykin, S., Newheart, A., Milla, M. A., & Condor, P. (2021). Prompt penetration and substorm effects over Jicamarca during the September 2017 geomagnetic storm. *Journal of Geophysical Research: Space Physics*, *126*, e2021JA029651. https://doi.org/10.1029/2021JA029651

Received 8 JUN 2021
Accepted 23 JUL 2021

Abstract We used reanalyzed Jicamarca radar measurements to study the response of equatorial ionospheric electrodynamics and spread F during the main phase of the large September 2017 geomagnetic storm. Our observations near dusk on 7 September show very large upward drifts followed by a large short-lived downward drift perturbation that completely suppressed the lower F region plasma irregularities and severely decreased the backscattered power from the higher altitude spread F. We suggest that this large short-lived westward electric field perturbation is most likely of magnetospheric origin and is due to a sudden and very strong magnetic field reconfiguration. Later in the early night period, data indicate large, mostly upward, drift perturbations generally consistent with standard undershielding and overshielding electric field effects, but with amplitudes significantly larger than expected. Our analysis suggests that occurrence of storm-time substorms is one of the major factors causing the large nighttime westward and eastward electric field perturbations observed at Jicamarca near the storm main phase. Our analysis also suggests that magnetospheric substorms play far more important roles on the electrodynamics of the equatorial nighttime ionosphere than has generally been thought.

1. Introduction

Geomagnetic storms drive low latitude ionospheric electric fields that strongly affect the distribution of ionospheric plasma density and the generation and evolution of equatorial plasma waves. Short time scale (less than a few hours) electric field perturbations occur mostly when large changes in magnetospheric convection, driven by large and rapid IMF Bz fluctuations, cause a temporary imbalance between region 1 and region 2 Birkeland currents (e.g., Chakrabarty et al., 2015; Fejer et al., 2007; Kikuchi et al., 2000; Spiro& Wolf, 1984; Spiro et al., 1988; Wolf et al., 1982; Wolf et al., 2007). This type of low-latitude electric fields was first unambiguously identified in data by Fejer et al. (1979) and Kelley et al. (1979), explained theoretically by Spiro et al. (1988) (although the actual phenomenon of penetration was demonstrated by Wolf and Jaggi (1973) and Jaggi and Wolf (1973) with numerical modeling), and were termed prompt penetration electric fields, a terminology followed in this paper as well. Other factors known to cause perturbations in the low-latitude electric fields are magnetospheric substorms (Chakrabarty et al., 2008; Huang, 2009, 2020; Kikuchi et al., 2000), solar wind dynamic pressure changes (Huang, 2020; Rout et al., 2019), solar flares (e.g., Zhang et al., 2017, 2019), and ULF waves (Huang, 2020). Longer time scale (up to a few days) electric field disturbances are mostly due to thermospheric disturbance wind dynamo effects (e.g., Blanc & Richmond, 1980; Scherliess & Fejer, 1997; Fejer et al., 2017; Navarro et al., 2019; Navarro & Fejer, 2020). The low latitude prompt penetration and disturbance dynamo electric fields vary as a function of local time but have basically opposite polarity (e.g., Fejer & Scherliess, 1997; Fejer, 2011).

The equatorial nighttime ionosphere often undergoes very large plasma density perturbations over a broad range of spatial and temporal scales generated by multistep processes including the collisional and collisionless Rayleigh-Taylor plasma instabilities (Aveiro & Hysell, 2010; Fejer & Kelley, 1980; Yokoyama & Stolle, 2017). Ionospheric electric fields play fundamentally important roles on the generation and evolution of these so-called equatorial spread F plasma irregularities primarily through their effects on the F-layer height (e.g., Fejer et al., 1999). This is especially the case near dusk and during geomagnetic storm main phases when the equatorial electric fields have their largest magnitudes (e.g., Fejer & Scherliess, 1997).

Intense equatorial spread F irregularities are associated with deep magnetic field-aligned large-scale plasma density depletions (bubbles). The nonlinear growth of equatorial plasma bubbles during their rapid height rise leads to the formation of kilometer scale plasma irregularities that affect low latitude communication and navigation systems (e.g., Groves et al., 1997). Storm-time equatorial plasma bubbles can often rise to very high altitudes and, therefore, significantly affect the nighttime ionosphere up to lower mid-latitudes (e.g., Abdu et al., 2007; Abdu, 2012).

The large and complex responses of the low and mid-latitude ionosphere to the September 2017 major geomagnetic storm has been recently examined in numerous detailed studies using Global Navigation Satellite Systems total electron content (GNSS TEC) receivers, radars, and ionosondes. Li et al. (2018) showed that strong southward IMF Bz excursions during this storm rapidly raised the F layer near sunset around the 120°E/60°W meridian region and lead to the development of intense equatorial plasma irregularities (plasma bubbles) extending to dip latitudes of ∼30°N and 46°N, respectively. Aa et al. (2018) presented postsunset intense plasma bubble observations over China and adjacent areas that reached up to ∼50°N (45.5°N magnetic), which corresponds to an equatorial mapped altitude of over 6,000 km. Aa et al. (2019) studied postsunset TEC depletions, associated with equatorial plasma bubbles (EPBs) that reached 46° magnetic latitudes and simultaneous mid-latitude traveling ionospheric disturbances (TIDs) over American sector. They suggested that the high altitude plasma depletions were driven by strong equatorial prompt penetration electric fields. Xiong et al. (2019) suggested that the opposite response of the low latitude ionosphere at Asian and American sectors during 2017 storm recovery phases was closely associated with the interplay of E region electrodynamics.

Rout et al. (2019) studied the large electric field disturbances in the equatorial ionosphere during the September 2017 geomagnetic storm using vertical drift measurements from the Jicamarca Radio Observatory (11°57' S, 76°51' W, dip latitude ∼0°), magnetic field observations from the equatorial electrojet over the Phillipines and from a latitudinal chain, and geosynchronous energetic electron fluxes from the Geostationary Operational Environmental Satellite 13 (GOES-13) over the North American sector. They pointed out that prompt penetration disturbance electric fields alone cannot account for the intense electric field perturbations over Jicamarca and that there were indications of significant substorm effects. Using Jicamarca incoherent scatter radar and magnetometer data over the Peruvian sector, Zhang et al. (2019) showed that the three X-class solar flares during the September 2017 storm caused very different electrodynamic effects and examined the disturbance dynamo effects during the storm recovery phase. Navarro and Fejer (2020) used Jicamarca drifts and thermospheric wind observations over Peru during this storm to study early phase prompt penetration and recovery phase long-lasting equatorial disturbance dynamo ionospheric effects.

De Paula et al. (2019) presented digisonde observations over São Luis (2.5°S, 44.3°W, 4.67° dip latitude) showing very large vertical and zonal plasma drift perturbations and strongly enhanced VHF and GPS S4 amplitude scintillations over the Brazilian equatorial region during the night of 07/08 September 2017. Alfonsi et al. (2021) examined the structuring and propagation of equatorial plasma bubbles in the Indian sector using an original method based on equatorial electrojet magnetic field variations. They inferred that these structures moved northward with a velocity of ∼650 m/s.

In this paper, we studied the response of the equatorial F-region ionosphere over Peru around the storm main phase on September 07/08, 2017 using detailed recently reanalyzed Jicamarca radar vertical drift and spread F measurements and complementary low and high latitude ionospheric and solar wind/magnetospheric activity indices. We note that we use the term prompt penetration to refer only to electric field of solar wind/magnetospheric origin associated with global changes in the high latitude convection. In the following sections, we first describe our measurement techniques, data analysis, and present our data. Then, we examine our results, and compare them with those from earlier studies. Finally, we discuss the implications of our results and summarize them.

2. Jicamarca Measurement Techniques and Data

We used Jicamarca incoherent scatter radar measurements from 16 LT (21 UT) on September 7, 2017 to 04 LT (09 UT) September 8, 2017. The drift measurements were reanalyzed in May 2021 to correct for occasional early night velocity aliasing resulting from very large drifts. The radar was operated in the oblique mode

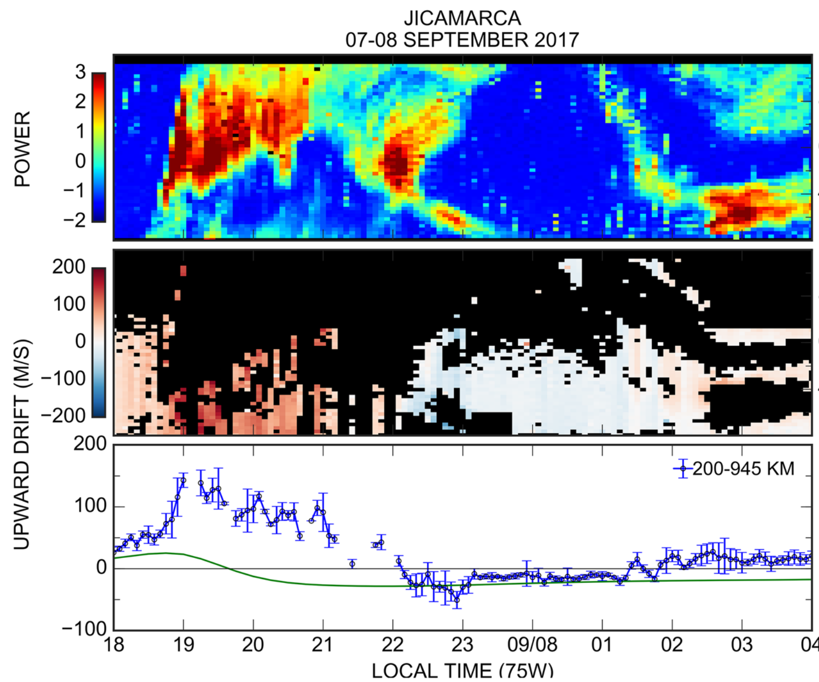

Figure 1. Coherent backscatter power in logarithmic scale, vertical drifts, and average drifts over Jicamarca during part of the September 7–8, 2017 storm main phase. The error bars denote the standard deviations on the averages. The green curve in the bottom panel shows the climatological quiet time pattern.

consisting of two experiments run simultaneously using time-division multiplexing and subdividing the main antenna. In this mode, plasma number density and electron and ion temperatures are measured using the north and south antenna quarters with beams directed a few degrees from magnetic field perpendicularity, while line-of-sight drifts are measured using quarters of the antenna with the beams directed about 2.4° eastward and 4.3° westward in the plane perpendicular to the magnetic field. We used the data acquisition and signal processing techniques described by Kudeki et al. (1999). The vertical (positive upward) and zonal plasma drifts (positive eastward) were derived from the line-of-sight drifts using the procedure described by Woodman (1970). The Jicamarca nighttime radar measurements in the plane perpendicular to the magnetic field also provide temporal and spatial information on the small-scale (3 meter) equatorial spread F irregularities. Ambient plasma drifts cannot be reliably obtained in strong spread F regions and when the plasma is strongly inhomogeneous in the east-west plane. During the September 2017 geomagnetic storm, plasma drifts and spread F irregularities were measured from 200 to 945 km with a 15 km range resolution and a 5 min integration time. Zonal drifts will not be considered in this study since their measurements had very large errors. Over Jicamarca an eastward electric field of 1 mV/m corresponds to an upward drifts of ~40 m/s.

Figure 1 presents an overview of radar observations during the period 7 September 23:00 UT–8 September 09:00 UT, which encompasses the first main phase of the geomagnetic storm (see also Figure 2). The two top panels show the coherent backscatter power from equatorial spread F irregularities measured by the west beam and the vertical plasma drift measurements. The third panel shows the average drifts obtained by deleting measurements with errors larger than 10 m/s and very large altitudinal variability. The error bars in Figure 1 correspond to the standard deviations on the average drifts, which were always larger than the measurement errors. Drift measurements at altitudes below 200 km are often less accurate and, therefore, they were not taken into account in our averages. Figure 1 shows the absence of plasma irregularities prior to about 1830 LT and vertical drifts increasing with time and nearly height independent below about 700 km, where the signal-to-noise ratios dropped below the level for accurate vertical drift measurements. After ~1840 LT, valley region irregularities (e.g., Hysell et al., 1990; Woodman & Chau, 2001), generated in the E region by the large storm-time electric fields, moved to higher altitudes with velocity of the ambient

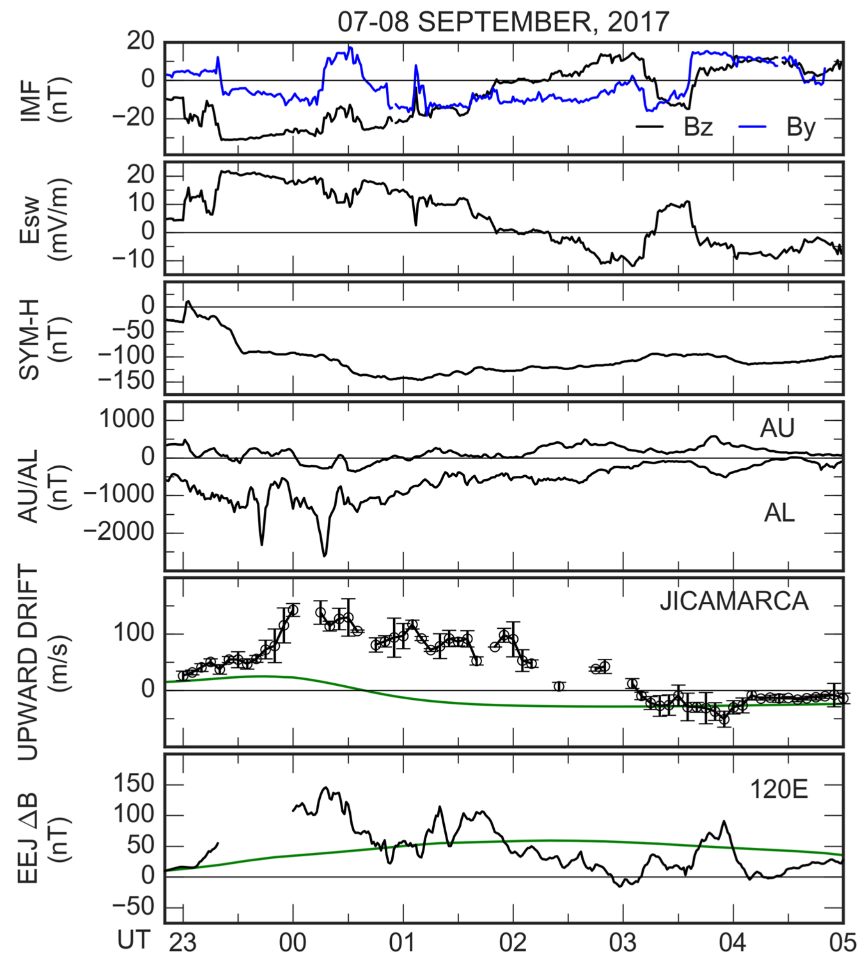

Figure 2. (From top to bottom) IMF Bz, IMF By, solar wind electric field, Symmetric H (SYM-H), auroral AU/AL indices, Jicamarca vertical drifts, and equatorial electrojet magnetic field magnitude over the Philippines during part of the September 2017 magnetic storm main phase. The green curves show the corresponding quiet time patterns, and error bars denote the standard deviations on the average drifts.

plasma. As the vertical drifts increased so did the altitudinal range of strong spread F echoes, which lead to fewer drift measurements.

Figure 1 shows a notable and rapid increase in the upward drifts from ∼1830–1900 LT (2330–0000 UT) leading to the rapid rise of spread F irregularities. This was followed by the sudden short-lived suppression plasma of irregularities below about 400 km and to a significant weakening of the backscattered power from the spread F irregularities at higher altitudes, which is indicative of a large downward drift (westward electric field) perturbation. Note that it is not possible to get an accurate estimate of the average vertical drifts from 1905 to 1910 LT due to the sparse and highly variable corresponding measurements. Nevertheless, we will point out later that our inferred large transient downward drift is fully consistent with a simultaneous large downward drift perturbation measured over the Brazilian equatorial region. Figure 1 also shows very large upward drifts with occasionally strong very short-lived downward drift perturbations between 2000 and 2200 LT. Intense spread F echoes and large vertical drift perturbations occurred up to about 2230 LT when the drifts reversed to downward leading to a short period without significant spread F activity. This was followed by a period of generally small upward drifts and increased spread F activity that lasted up to about sunrise. We now proceed to compare our results with those from earlier studies and to examine in more detail our results during 1800–2200 LT (2300–0300 UT) when storm-time effects over Jicamarca were the strongest.

3. Storm-Time Equatorial Electric Fields

The September 2017 large geomagnetic storm started at ~2345 UT on the 6th with the arrival of the first of two interplanetary coronal mass ejections (ICMEs) and ended at ~1900 UT on 8th. The first main phase, which lasted from 2130 UT on the 7th up to ~0200 UT on the 8th, was significantly strengthened by the arrival of the shock-driven second ICME at ~2300 UT. During this main phase, the Sym-H geomagnetic index reached a minimum of −146 nT at 0108 UT on the 8th and the AU/AL auroral electrojet indices had large variations. Ionospheric and thermospheric effects during and after this large storm were discussed in detail in numerous publications (e.g., Aa et al., 2018; Alfonsi et al., 2021; De Paula et al., 2019; Navarro & Fejer, 2020; Rout et al., 2019; Xiong et al., 2019; Zhang et al., 2019).

To put the observations into the context of geomagnetic conditions, Figure 2 presents the Jicamarca height averaged vertical drifts (same as in Figure 1), now as a function of UT, with overlayed values of the GSM Y and Z components of the interplanetary magnetic field (IMF), Y(east-west) component of the motional solar wind electric field, and geomagnetic indices SYM-H and AU/AL. Solar wind and IMF values are 5 min averages time-propagated to the noon magnetopause location obtained from the NASA OMNI database. In addition, Figure 2 presents the estimated strength of the equatorial electrojet obtained from the horizontal component of ground-based magnetic field data over the Philippines derived by subtracting from the 5 min measurements over Davao (7.1°N, 125.6°E, dip angle −0.3°) the corresponding values from Manila (14.6°N, 121°E, dip angle 16.8°). For a given local time location, the strength of the daytime equatorial electrojet is proportional to the vertical drift velocity. The average quiet daytime upward drifts over the Philippines are ~20 m/s (Fejer et al., 2008a), which correspond to eastward electric fields of ~0.5 mV/m. Over these two sites, equatorial prompt penetration electric fields driven by global convection changes should have the same polarity and comparable magnitudes up to ~02–03 UT due to the 13 h of difference in local time (e.g., Fejer & Scherliess, 1997; Fejer et al., 2008b; Sazykin, 2000).

Figure 2 shows a rapid increase of the upward drifts during ~2330–0000 UT (1830–1900 LT) even as the interplanetary electric field was decreasing slowly. In this period, the auroral electrojet indices exhibited large variations. From ~0000 UT to ~0020 UT, the IMF Bz underwent a northward and then a southward excursion that was associated with large changes in the solar wind electric fields and AU/AL indices. The IMF By also sharply changed signs. Over this period, the sharp drop in the radar backscattered power precluded accurate Jicamarca drift estimates while the Philippines equatorial electrojet magnetic field data underwent only a small decrease from its storm-driven increased average value of ~100 nT. From ~0020 UT to ~0200 UT, the solar wind zonal electric fields decreased slowly, except for faster decreases at ~0115 UT and ~0145 UT. The corresponding equatorial electrodynamic perturbations over these sites are generally consistent with southward Bz-driven undershielding eastward electric fields, but often with magnitudes significantly different than expected. During ~01–02 UT, for example, the Jicamarca and electrojet data estimated eastward electric field perturbations are ~2 mV/m and ~0.5 mV/m, respectively. The IMF Bz northward turning at 02 UT led to eastward and westward overshielding electric fields over Peru and the Philippines, respectively, but again with much different magnitudes than expected from prompt penetration effects. We note that the transition from undershielding to overshielding conditions at Jicamarca generally occurs at ~02–03 UT (21–22 LT) (e.g., Fejer & Scherliess, 1997; Fejer et al., 2008b; Sazykin, 2000), although the exact local time depends on the season and solar flux level. After ~06 UT, Figure 1 shows smaller eastward and westward electric field perturbations in the postmidnight and daytime sectors, respectively, which are typical of disturbance dynamo vertical drift and electrojet current effects (e.g., Rout et al., 2019; Scherliess & Fejer, 1997).

Figure 3 shows in the top three panels the solar wind electric field now taking into account the propagation time from the magnetopause to the equatorial ionosphere, the AU and AL auroral indices, and again the Jicamarca average drifts. The bottom panel shows the digisonde derived vertical drifts over São Luís (2.5°S, 44.3°W, − 4.67° dip latitude), Brazil presented by De Paula et al. (2019). These digisonde drifts had a 10 min resolution and, therefore, they have likely underestimated the vertical drift decrease at ~0000 UT (2100 LT), which was related to the large and sharp backscattered power decrease over Jicamarca. Figure 3 indicates that after 0010 UT the disturbance drifts over Jicamarca generally retained their large eastward values up to ~0200–0300 UT even as the solar wind was decreasing systematically. After the decrease of the digisonde from 60 m/s upward at 2350 UT (2050 LT) on the 7th to 30 m/s downward at 0010 UT (2110 LT),

10.1029/2021JA029651

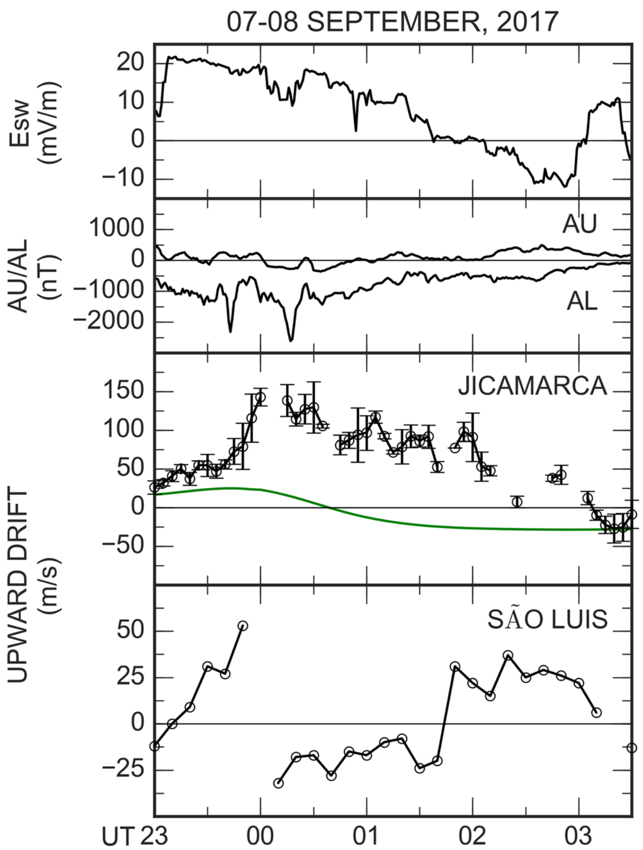

Figure 3. Solar wind electric fields, AU/AL auroral indices, Jicamarca average vertical drifts and digisonde derived drifts over São Luis, Brazil near the main phase of the 2017 September geomagnetic storm.

they remained downward up to ~0145 UT (2245 LT), in sharp contrast to the Jicamarca drifts. However, these latter measurements were made when the F layer was below ~300 km and, therefore, significantly affected by chemical processes. Nevertheless, even under these unfavorable measuring conditions, the digisonde would have detected upward drifts if there had been large overshielding electric fields over São Luís. These data indicates the occurrence of a large zonal electric field gradient over South America from ~0010 to 0145 UT. The digisonde drifts reversed to upward as the IMF Bz turned northward indicating overshielding conditions, reached values of ~20 m/s up to ~0300 UT, and turned downward again at ~0315 UT, at about the same time as the Jicamarca drifts.

Abdu et al. (2009) showed that, even under southward Bz conditions, the evening prereversal enhancements in the equatorial upward drifts and the consequent equatorial spread F generation can be fully inhibited by large westward prompt penetration electric fields during overshielding events. Rout et al. (2019) pointed out that the IMF Bz was already southward prior to the arrival of the shock-driven second ICME at about 2300 UT that triggered a large substorm-like variation in the AL index with a peak value of ~2,500 nT. The intensification of the AL index was accompanied by simultaneous electron injections detected by geosynchronous GOES-13 satellite at 75°W near the Jicamarca sector. Rout et al. concluded that prior to 00 UT on the 8th there were strong substorm driven eastward electric fields in addition to the storm time prompt penetration undershielding electric fields. We will show later that substorms can significantly increase the prereversal drift velocities even during periods of relatively modest levels of geomagnetic activity and small solar wind electric fields. Since the penetration efficiency of solar wind electric fields near sunset is higher than during the day (e.g., Fejer & Scherliess, 1997; Fejer et al., 2008b), during large geomagnetic storms it is usually very difficult to determine the relative contributions from substorm electric fields to the disturbance vertical drifts near dusk.

We have seen that although the equatorial data during this event have general features consistent with the effects of standard prompt penetration electric fields, there were also a number of unexplained results. The large westward electric field effects at 00 UT over Peru, the corresponding large decrease of the radar backscattered power, and the large discrepancies in the amplitudes of the dayside and night side disturbance electric fields and their relationship to the solar wind electric fields, all strongly indicate the importance of additional electric field driving processes was not limited to the prereversal enhancement period discussed by Rout et al. (2019). The GOES-13 data presented by Rout et al. (2019) data shows several electron injections including on the 8th, which further strongly suggests that substorms perhaps related to the large IMF By changes also made significant contributions to the large equatorial vertical drift fluctuations near the storm main phase. This will be discussed further later. Clearly, this highly complex storm significantly affected the equatorial ionosphere through the combined effects of various solar wind, magnetospheric and ionospheric disturbance processes.

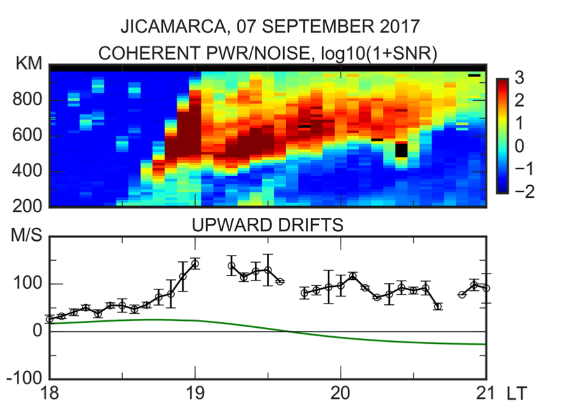

Figure 4. Coherent backscattered power from the 3-m irregularities and height averaged vertical drifts over Jicamarca during the period of strongest September 2017 storm effects. The green curve corresponds to the quiet time pattern and the error bars denote the standard deviations from the average drifts.

4. Effects on Equatorial Spread F Irregularities

We have seen that there were large and highly variable vertical drifts and strong spread F over Jicamarca close to the September 2017 storm main phase. Figure 4 shows the coherent backscattered power from the west

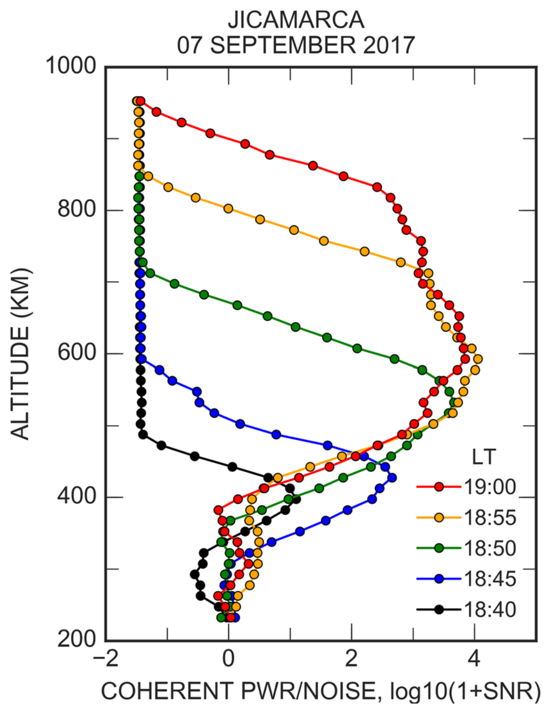

Figure 5. Temporal and initial altitudinal variations of the coherent backscattered power from the Jicamarca 3-m irregularities during their initial growth phase.

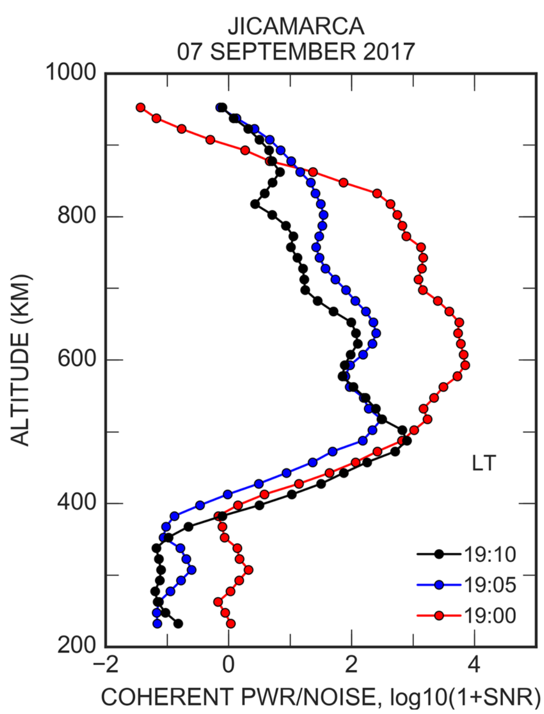

Figure 6. Variation of the coherent backscattered power decrease after the large downward drift perturbation at 1900 LT.

beam and the corresponding vertical drifts during the period of strongest storm effects. There were only small differences between coherent power height profiles measured by the east and west beams up to about midnight (0500 UT). Figure 4 illustrates the rapid initial rise of the 3-m irregularities with the increasing upward drifts and the large decrease in the backscattered power at ~1900LT (0000 UT). Later, the coherent power and the vertical drifts were highly variable and there were also strong altitudinal variations on the backscattered power. As discussed below, the gaps in the drift measurements and the associated sharp decreases in the backscattered power are indicative of large downward drift perturbations.

We have used the time rate of change of the height of the backscattered power from the 3-m irregularities to infer the initial motion of the corresponding large-scale equatorial plasma bubbles (depletions). Figure 5 indicates that the inferred irregularity rise velocities vary from about 200 to 550 m/s, which are much larger than the rapidly increasing measured ambient upward drifts (see Figure 4), and that these rise velocities did not increase monotonically. Figure 5 also illustrates in more detail the large dynamic range of the backscatter power from the 3-m spread F irregularities measured the Jicamarca radar, even with reduced gain from 4-way radar beam splitting.

The growth rates and rise velocities of the convective interchange instability driven equatorial spread F and corresponding plasma depletions are determined mainly by their gravitational (g/υ_{in}, where g is gravity and υ_{in} is the ion-neutral collisional frequency) and electrodynamic (E/B, where E is the ambient electric field perpendicular to the magnetic field B) components (e.g., Aveiro & Hysell, 2010; Keskinen et al., 2003; Ossakow & Chaturvedi, 1978; Yokoyama & Stolle, 2017). Since the gravitational term g/υ_{in} varies from ~40 m/s at 350 km to ~220 m/s at 450 km, for example, the electric field (or vertical drift) rarely makes a significant contribution to the bubble rise velocity and growth rate, except at the lowest altitudes. Therefore, once these irregularities are generated, even large westward electric fields (downward drifts) cannot damp them out, except at the lowest altitudes.

Figure 6 shows in more detail that ~19 LT (00 UT) the very weak bottomside irregularities disappeared and that the intensity of the backscattered power intensity decreased significantly below 850 km (sharp vertical effect on upper plot in Figure 4) while it increased at higher altitudes. We note that the large power decrease between ~500–800 km resulted from the largely decreased growth rates of lower altitude irregularities that were convected upward. The backscattered power below ~400 km at 1905 LT was at about the minimum detectable level for accurate drift measurements. Figure 6 also indicates the development of plasma bubble structuring after 1900 LT. As these irregularities rapidly drift upward, their structuring is also strongly affected by their large and highly variable westward storm-time drifts. We note that spread F over Jicamarca would have been more severely affected if the large downward drift had occurred earlier.

De Paula et al. (2019) showed that the large downward drift over São Luis at 2100 LT (0000 UT) shown in Figure 3 did not suppress the overhead range spread F (indicative of plasma bubbles) either. On the other hand, it significantly decreased the strong VHF (240 MHz) and GPS

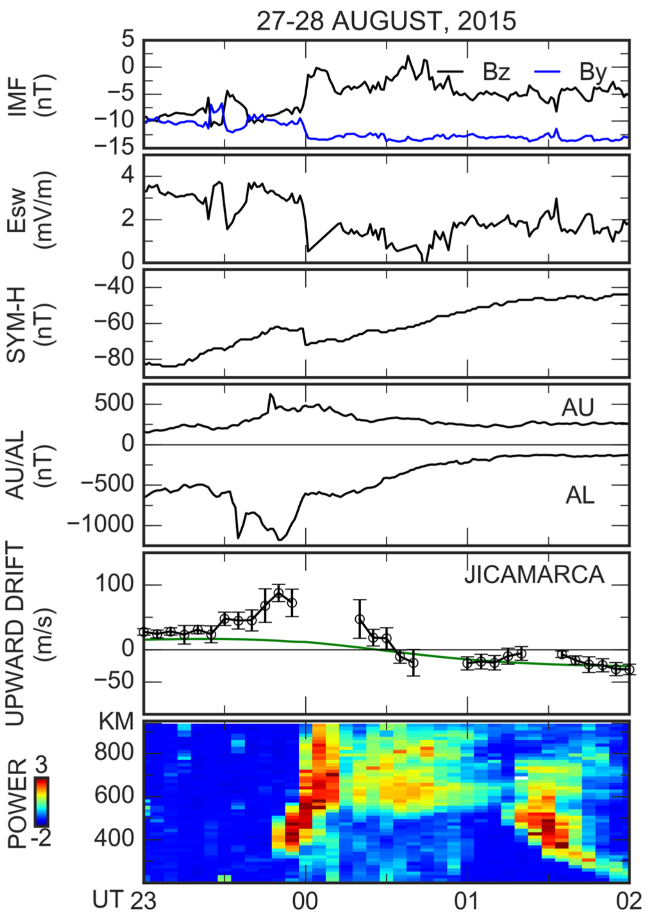

Figure 7. Solar wind and magnetospheric indices and average Jicamarca vertical drifts and coherent backscattered power during August 27–28, 2015. The green line corresponds to the quiet drift pattern. The errors bars denote the errors of the measurements or the standard deviations of their drift variability whichever is larger.

(1,227.60 MHz and 1,575.4 MHz) amplitude scintillations that at started at 2300 UT with the storm sudden commencement.

5. Discussion

We have examined some the major equatorial ionospheric electrodynamic disturbances over Jicamarca, the Phillipines and Brazil around the September 2017 storm main phase. The observed evening and early night large vertical drift perturbations are generally consistent with strong prompt penetration driven undershielding and overshielding effects, but they also exhibit major features strongly suggesting the importance of additional driving processes. Rout et al. (2019) suggested that substorms played an important role on the very large eastward electric fields over Jicamarca before ~00 UT on the 8th. Our more extensive data is consistent with this suggestion, but it also strongly indicates that substorms likely also drove large, mostly eastward, zonal electric fields over Jicamarca up to ~03 UT on 8 September.

Magnetospheric substorms are known to drive eastward and westward low latitude electric field perturbations (Hashimoto et al., 2017; Hui et al., 2017; Huang, 2012, 2020; Kikuchi et al., 2003). Storm time substorms often shows a quasi-periodicity of ~3 h associated with the so-called sawtooth events, (e.g., Reeves, et al., 2003). In these events, substorm onsets cause dayside eastward electric fields, except when they are associated with northward Bz turnings (e.g., Tulasi Ram et al., 2017; Huang, 2020). During strong geomagnetic storms, when IMF Bz is large and southward, the strong polar-to-equator electrodynamic coupling makes it difficult to determine the substorm electric field contribution (e.g., Chakrabarty et al., 2008).

To emphasize the complexity of response, we provide another event example. Late in August 2015 there was a period of moderate recurrent geomagnetic activity with relatively small (below 5 mV/m) solar wind electric fields and AE indices of ~500 nT. Figure 7 presents solar wind, magnetospheric, and ionospheric parameters, and Jicamarca vertical drifts close to dusk during August 27, 2015. In this period, some drift measurements (e.g., around ~0000 UT) had again large errors and altitudinal variability and, therefore, often precluded the derivation of accurate vertical drifts. Figure 7 shows that initially the upward drifts were generally close to their small quiet-time climatological values. They started increasing strongly at ~2325 UT when both the solar wind electric fields (~3 mV/m) were typically too small for directly driving noticeable equatorial prompt penetration electric fields. The upward drifts first increased at ~2320 UT and even more strongly at ~2345 UT with the onsets of large substorms, as indicated by the AU and AL indices. This resulted in the largest dusk side upward drift perturbation (~60 m/s) ever recorded over Jicamarca during June solstice. In the present case, the dusk side equatorial electric field and the solar wind electric field had comparable values, and the IMF By was essentially constant at ~12 nT. The backscattered power decreased strongly at ~00UT, which suggests a large decrease in the upward drifts were associated with the substorm recovery. Later, upward drifts reached a peak value of ~30 m/s at ~0020 UT, and underwent small upward and downward perturbations thereafter. The Jicamarca database has other examples of large sudden duskside decreases of increases and decreases in the evening vertical and sudden decreases in spread F backscattered power drifts associated with substorm activity similar to that shown in Figure 7.

The results in Figure 7 further supports the suggestion that substorms were major drivers of the large eastward and westward electric field disturbances over Jicamarca during the September 2017 storm main phase. The standard prompt penetration mechanism is clearly unable to fully account for our observations. Chakrabarty et al. (2017) suggested that IMF B_y changes under southward IMF B_z can cause distortion of the

DP2 cells and the rotation of the electrodynamical boundary between the dawn and dusk cells. We speculate that that this large dusk westward electric field occurred through the rapid dipolarizations of magnetotail field lines (e.g., Kokubun & McPherron, 1981; Wolf et al., 1982; Fejer et al., 1990) during the recovery of the IMF By associated substorm. This configuration change of the magnetic field has been explained as resulting from a diversion of the well-developed cross-tail currents into the polar ionosphere (e.g., Ebihara et al., 2014).

The large evening and early night zonal electric fields (up to ∼4 mV/m) measured by the Jicamarca radar during 7–8 September must have been associated with significantly larger values at higher latitudes. Mozer (1970) showed that, for a dipole centered geomagnetic field with equipotential field lines, the zonal ionospheric projection of an electric field independent of the radial distance in the equatorial plane varies as $L^{3/2}$. This is in generally good agreement with experimental observations and Rice Convection model simulations of prompt penetration electric fields (e.g., Fejer et al., 1990; Sazykin, 2000). The longitudinal and latitudinal variations of substorm electric fields are not well known at present and neither is their solar flux dependence. Hashimoto et al. (2020) suggested that substorms may play crucial roles in driving strong overshielding electric fields in the nightside midlatitude ionosphere. Our results indicate that storm time substorms are likely play important roles in the nighttime equatorial ionosphere as well. Clearly, additional plasma drift (electric field) observations as well as thermospheric wind measurements over a range of latitude and longitudes combined with more detailed modeling studies will be required for a more detailed understanding of the response of the ionosphere to geomagnetic activity.

6. Summary and Conclusions

The September 2017 geomagnetic storm caused very large and complex ionospheric disturbances extending from polar to equatorial latitudes. These disturbances, driven by strong and highly variable thermospheric winds and electric fields and dynamic pressure changes, covered a very broad range of temporal and spatial scales and were particularly severe in the nighttime low and equatorial ionosphere.

We have seen that substorms can drive large eastward dusk-side equatorial electric fields. We noted that at ∼0000 UT on the 8th there were very large westward electric field perturbations in the eastern Brazilian equatorial region and only a very minor equatorial westward electric field perturbation over the Philippines. We suggest that large westward electric field resulted from a very fast and strong magnetotail dipolarization. This large electric field briefly completely damped the low altitude plasma irregularities significantly decreased the spread F backscattering power at higher altitudes. After about 0000 UT on the 8th, the nighttime and daytime electrodynamic perturbations over Jicamarca and the Phillipines were generally consistent with prompt penetration electric field effects, but that was not the case for the ratios of their magnitudes. This further suggests that the nighttime large upward electric fields were significantly enhanced first by undershielding and then by overshielding substorm electric fields. Our results fully confirm that, particularly during storms, it is difficult to determine the relative importance of substorm electric fields at equatorial latitudes. They also strongly suggest that substorm electric fields play significantly more important roles in the electrodynamics of the equatorial ionosphere than has been previously acknowledged.

The potential occurrence of significant storm-time nighttime substorm electric fields at equatorial latitudes would raise important questions on the relative importance of various electric field disturbance processes. Currently all but one empirical equatorial electric field model and all simulation studies account for only one storm time driving mechanism. Clearly, more extensive measurements of basic physical parameters and modeling studied are needed for deeper understanding of the various complex low latitude ionospheric processes during geomagnetic storms.

Data Availability Statement

The radar data are available at the website of the Jicamarca Radio Observatory (http://jro.igp.gob.pe), the geomagnetic indices are available from the World Data Center for Geomagnetism Kyoto (http://wdc.kugi.kyoto-u.ac.jp) and from the National Centers for Environmental Information of the National Oceanic and

Atmospheric Administration (https://www.ngdc.noaa.gov), and the solar wind data from the Space Physics Data Facility (https://omniweb.gsfc.nasa.gov). We thank the Jicamarca staff for the radar operations.

Acknowledgments
We thank Phil Erickson for helpful comments and corrections. The work at Utah State was supported by the NASA H-LWS program through grant 80NSSC17K071. The work at Rice was supported by the NASA grants 80SS-C17K071 and 80NSS20K1512, and the NASA grant AGS-134072. The Jicamarca Radio Observatory is a facility of the Instituto Geofisico del Peru operated with support from NSF award AGS-1732209 through Cornell University.

References

Aa, E., Huang, W., Liu, S., Ridley, A., Zou, S., Shi, L., et al. (2018). Midlatitude plasma bubbles over China and adjacent areas during a magnetic storm on 8 September 2017. *Space Weather*, *16*(3), 321–331. https://doi.org/10.1002/2017SW001776

Aa, E., Zou, S., Ridley, A., Zhang, S., Coster, A. J., Erickson, P. J., et al. (2019). Merging of storm time midlatitude traveling ionospheric disturbances and equatorial plasma bubbles. *Space Weather*, *17*, 285–298. https://doi.org/10.1029/2018sw002101

Abdu, M. A. (2012). Equatorial spread F/plasma bubble irregularities under storm time disturbance electric fields. *Journal of Atmospheric and Solar-Terrestrial Physics*, *75–76*, 44–56. https://doi.org/10.1016/j.jastp.2011.04.024

Abdu, M. A., Kherani, E. A., Batista, I. S., & Sobral, J. H. A. (2009). Equatorial evening prereversal vertical drift and spread F suppression by disturbance penetration electric fields. *Geophysical Research Letters*, *36*, L19103. https://doi.org/10.1029/2009gl039919

Abdu, M. A., Maruyama, T., Batista, I. S., Saito, S., & Nakamura, M. (2007). Ionospheric responses to the October 2003 superstorm: Longitude/local time effects over equatorial low and middle latitudes. *Journal of Geophysical Research*, *112*, A10306. https://doi.org/10.1029/2006ja012228

Alfonsi, L., Cesaroni, C., Spogli, L., Regi, M., Paul, A., Ray, S., et al. (2021). Ionospheric disturbances over the indian sector during 8 September 2017 geomagnetic storm: plasma structuring and propagation. *Space Weather*, *19*(3). https://doi.org/10.1029/2020SW002607

Aveiro, H. C., & Hysell, D. L. (2010). Three-dimensional numerical simulation of equatorial F-region plasma irregularities with bottomside shearflow. *Journal of Geophysical Research*, *115*, A11321. https://doi.org/10.1029/2010JA015602

Blanc, M., & Richmond, A. D. (1980). The ionospheric disturbance dynamo. *Journal of Geophysical Research*, *85*(A4), 1669–1686. https://doi.org/10.1029/JA085iA04p01669

Chakrabarty, D., Hui, D., Rout, R., Sekar, R., Bhattacharyya, A., Reeves, G. D., & Ruohoniemi, J. M. (2017). Role of IMFBy in the prompt electric field disturbances over equatorial ionosphere during a space weather event. *Journal of Geophysical Research Space Physics*, *122*, 2574–2588. https://doi.org/10.1002/2016JA022781

Chakrabarty, D., Rout, D., Sekar, R., Narayanan, R., Reeves, G. D., Pant, T. K., et al. (2015). Three different types of electric field disturbances affecting equatorial ionosphere during a long-duration prompt penetration event. *Journal of Geophysical Research: Space Physics*, *120*(6), 4993–5008. https://doi.org/10.1002/2014JA020759

Chakrabarty, D., Sekar, R., Sastri, J. H., & Ravindran, S. (2008). Distinctive effects of interplanetary electric field and substorm on nighttime equatorial F layer: A case study. *Geophysical Research Letters*, *35*, L19108. https://doi.org/10.1029/2008GL035415

De Paula, E. R., de Oliveira, C. B. A., Caton, R. G., Negreti, P. M., Batista, I. S., Martinon, A. R. F., et al. (2019). Ionospheric irregularity behavior during the September 6–10, 2017 magnetic storm over Brazilian equatorial–low latitudes. *Earth, Planets and Space*, *71*, 42. https://doi.org/10.1186/s40623-019-1020-z

Ebihara, Y., Tanaka, T., & Kikuchi, T. (2014). Counter equatorial electrojet and overshielding after substorm onset: Global MHD simulation study. *Journal of Geophysical Research: Space Physics*, *119*(9), 7281–7296. https://doi.org/10.1002/2014JA020065

Fejer, B. G. (2011). Low latitude ionospheric electrodynamics. *Space Science Reviews*, *158*(1), 145–166. https://doi.org/10.1007/s11214-010-9690-7

Fejer, B. G., Blanc, M., & Richmond, A. D. (2017). Post-storm middle and low-latitude ionospheric electric fields effects. *Space Science Reviews*, *206*(1–4), 407–429. https://doi.org/10.1007/s11214-016-0320-x

Fejer, B. G., Gonzales, C. A., Farley, D. T., Kelley, M. C., & Woodman, R. F. (1979). Equatorial electric fields during magnetically disturbed conditions 1. The effect of interplanetary magnetic field. *Journal of Geophysical Research*, *84*(A10), 5797. https://doi.org/10.1029/JA084iA10p05797

Fejer, B. G., Jensen, J. W., Kikuchi, T., Abdu, M. A., & Chau, J. L. (2007). Equatorial ionospheric electric fields during the November 2004 magnetic storm. *Journal of Geophysical Research*, *112*, A10304. https://doi.org/10.1029/2007JA012376

Fejer, B. G., Jensen, J. W., & Su, S.-Y. (2008a). Quiet time equatorial F region vertical plasma drift model derived from ROCSAT-1 observations. *Journal of Geophysical Research*, *113*, A05304. https://doi.org/10.1029/2007JA012801

Fejer, B. G., Jensen, J. W., & Su, S.-Y. (2008b). Seasonal and longitudinal dependence of equatorial disturbance vertical plasma drifts. *Geophysical Research Letters*, *35*(20). https://doi.org/10.1029/2008GL035584

Fejer, B. G., & Kelley, M. C. (1980). Ionospheric irregularities. *Reviews of Geophysics*, *18*(2), 401–454. https://doi.org/10.1029/RG018i002p00401

Fejer, B. G., & Scherliess, L. (1997). Empirical models of storm time equatorial zonal electric fields. *Journal of Geophysical Research: Space Physics*, *102*(A11), 24047–24056. https://doi.org/10.1029/97JA02164

Fejer, B. G., Scherliess, L., & de Paula, E. R. (1999). Effects of the vertical plasma drift velocity on the generation and evolution of equatorial spread F. *Journal of Geophysical Research*, *104*(A9), 19859–19869. https://doi.org/10.1029/1999JA900271

Fejer, B. G., Spiro, R. W., Wolf, R. A., & Foster, J. C. (1990). Latitudinal variation of perturbation electric fields during magnetically disturbed periods-1986 SUNDIAL observations and model results. In *Annales Geophysicae* (*8*, pp. 441–454).

Groves, K. M., Basu, S., Weber, E. J., Smitham, M., Kuenzler, H., Valladares, C., et al. (1997). Equatorial scintillation and systems support. *Radio Science*, *32*, 2047–2064. https://doi.org/10.1029/97RS00836

Hashimoto, K. K., Kikuchi, T., Tomizawa, I., Hosokawa, K., Chum, J., Buresova, D., et al. (2020). Penetration electric fields observed at middle and low latitudes during the 22 June 2015 geomagnetic storm. *Earth, Planets and Space*, *72*(1), 71. https://doi.org/10.1186/s40623-020-01196-0

Hashimoto, K. K., Kikuchi, T., Tomizawa, I., & Nagatsuma, T. (2017). Substorm overshielding electric field at low latitude on the nightside as observed by the HF Doppler sounder and magnetometers. *Journal of Geophysical Research: Space Physics*, *122*(10), 10851–10863. https://doi.org/10.1002/2017JA024329

Huang, C.-S. (2009). Eastward electric field enhancement and geomagnetic positive bay in the dayside low-latitude ionosphere caused by magnetospheric substorms during sawtooth events. *Geophysical Research Letters*, *36*, L18102. https://doi.org/10.1029/2009GL040287

Huang, C.-S. (2012). Statistical analysis of dayside equatorial ionospheric electric fields and electrojet currents produced by magnetospheric substorms during sawtooth events. *Journal of Geophysical Research*, *117*, A02316. https://doi.org/10.1029/2011JA017398

Huang, C.-S. (2020). Systematical analyses of global ionospheric disturbance current systems caused by multiple processes: Penetration electric fields, solar wind pressure impulses, magnetospheric substorms, and ULF waves. *Journal of Geophysical Research: Space Physics*, *125*, e2020JA027942. https://doi.org/10.1029/2020JA027942
Hui, D., Chakrabarty, D., Sekar, R., Reeves, G. D., Yoshikawa, A., & Shiokawa, K. (2017). Contribution of storm time substorms to the prompt electric field disturbances in the equatorial ionosphere. *Journal of Geophysical Research: Space Physics*, *122*, 5568–5578. https://doi.org/10.1002/2016JA023754
Hysell, D. L., Kelley, M. C., Swartz, W. E., & Woodman, R. F. (1990). Seeding and layering of equatorial spread by gravity waves. *Journal of Geophysical Research*, *95*(17), 253. https://doi.org/10.1029/JA095iA10p17253
Jaggi, R. K., & Wolf, R. A. (1973). Self-consistent calculation of the motion of the sheet of ions in the magnetosphere. *Journal of Geophysical Research*, *78*(16), 2852–2866. https://doi.org/10.1029/ja078i016p02852
Kelley, M. C., Fejer, B. G., & Gonzales, C. A. (1979). An explanation for anomalous equatorial ionospheric electric field associated with a northward turning of the interplanetary magnetic field. *Geophysical Research Letters*, *6*, 301–304. https://doi.org/10.1029/GL006i004p00301
Keskinen, M. J., Ossakow, S. L., & Fejer, B. G. (2003). Three-dimensional nonlinear evolution of equatorial spread-F bubbles. *Geophysical Research Letters*, *30*(16), 1855. https://doi.org/10.1029/2003GL017418
Kikuchi, T., Hashimoto, K. K., Kitamura, T.-I., Tachihara, H., & Fejer, B. (2003). Equatorial counterelectrojets during substorms. *Journal of Geophysical Research: Space Physics*, *108*(A11), 1406. https://doi.org/10.1029/2003JA009915
Kikuchi, T., Lühr, H., Schlegel, K., Tachihara, H., Shinohara, M., & Kitamura, T.-I. (2000). Penetration of auroral electric fields to the equator during a substorm. *Journal of Geophysical Research*, *105*(A10), 23251–23261. https://doi.org/10.1029/2000JA900016
Kokubun, S., & McPherron, R. L. (1981). Substorm signatures at synchronous altitude. *Journal of Geophysical Research*, *86*, 11265–11277. https://doi.org/10.1029/JA086iA13p11265
Kudeki, E., Bhattacharyya, S., & Woodman, R. F. (1999). A new approach in incoherent scatter F region E×B drift measurements at Jicamarca. *Journal of Geophysical Research*, *104*(A12), 28145–28162. https://doi.org/10.1029/1998JA900110
Li, G., Ning, B., Wang, C., Abdu, M. A., Otsuka, Y., Yamamoto, M., et al. (2018). Storm-enhanced development of postsunset equatorial plasma bubbles around the meridian 120°E/60°W on 7–8 September 2017. *Journal of Geophysical Research: Space Physics*, *123*, 7985–7998. https://doi.org/10.1029/2018JA025871
Mozer, F. S. (1970). Electric field mapping in the ionosphere at the equatorial plane. *Planetary and Space Science*, *18*(2), 259–263. https://doi.org/10.1016/0032-0633(70)90161-3
Navarro, L. A., & Fejer, B. G. (2020). Storm-time coupling of equatorial nighttime F-region neutral winds and plasmas drifts. *Journal of Geophysical Research: Space Physics*, *125*, e2020JA028253. https://doi.org/10.1029/2020JA028253
Navarro, L. A., Fejer, B. G., & Scherliess, L. (2019). Equatorial disturbance dynamo vertical plasma drifts over Jicamarca: Bimonthly and solar cycle dependence. *Journal of Geophysical Research: Space Physics*, *124*, 4833–4841. https://doi.org/10.1029/2019JA026729
Ossakow, S. L., & Chaturvedi, P. K. (1978). Morphological studies of rising equatorial spread F bubbles. *Journal of Geophysical Research: Space Physics*, *83*(A5), 2085–2090. https://doi.org/10.1029/JA083iA05p02085
Reeves, G. D., Henderson, M. G., Skoug, R. M., Thomsen, M. F., Borovsky, J. E., Funtsen, H. O., et al. (2003). Image, polar, and geosynchronous observations of substorm and ring current ion injection. In *Disturbances in geospace: The storm-substorm relationship*. (pp. 91–101). American Geophysical Union (AGU). https://doi.org/10.1029/142GM09
Rout, D., Pandey, K., Chakrabarty, D., Sekar, R., & Lu, X. (2019). Significant electric field perturbations in low latitude ionosphere due to the passage of two consecutive ICMEs during 6–8 September 2017. *Journal of Geophysical Research: Space Physics*, *124*(11), 9494–9510. https://doi.org/10.1029/2019JA027133
Sazykin, S. (2000). *Theoretical studies of penetration of magnetospheric electric fields to the ionosphere* [PhD thesis, Utah State University, Logan, UT]. https://digitalcommons.usu.edu/etd/7152/
Scherliess, L., & Fejer, B. G. (1997). Storm time dependence of equatorial disturbance dynamo zonal electric fields. *Journal of Geophysical Research*, *102*(24)–24037. https://doi.org/10.1029/97JA02165
Spiro, R. W., & Wolf, R. A. (1984). Electrodynamics of convection in the inner magnetosphere. In *Magnetospheric currents*. (pp. 247–259). American Geophysical Union (AGU). https://doi.org/10.1029/GM028p024710.1029/gm028p0247
Spiro, R. W., Wolf, R. A., & Fejer, B. G. (1988). Penetration of high-latitude-electric-field effects to low latitudes during SUNDIAL 1984. *Annales Geophysicae*, *6*, 39–50.
Tulasi Ram, S., Ajith, K. K., Yokoyama, T., Yamamoto, M., & Niranjan, K. (2017). Vertical rise velocity of equatorial plasma bubbles estimated from Equatorial Atmosphere Radar (EAR) observations and HIRB model simulations. *Journal of Geophysical Research: Space Physics*, *122*, 6584–6594. https://doi.org/10.1002/2017JA024260
Wolf, R. A., Harel, M., Spiro, R. W., Voigt, G.-H., Reiff, P. H., & Chen, C.-K. (1982). Computer simulation of inner magnetospheric dynamics for the magnetic storm of July 29, 1977. *Journal of Geophysical Research*, *87*(A8), 5949–5962. https://doi.org/10.1029/JA087iA08p05949
Wolf, R. A., & Jaggi, R. K. (1973). Can the magnetospheric electric field penetrate to the low-latitude ionosphere? *Comments Astrophysical Space Science*, *5*(4), 99–107.
Wolf, R. A., Spiro, R. W., Sazykin, S., & Toffoleto, F. R. (2007). How the Earth's inner magnetosphere works: An evolving picture. *Journal of Atmospheric and Solar Terrestrial Physics*, *69*(3), 288–302. https://doi.org/10.1016/j.jastp.2006.07.026
Woodman, R. F. (1970). Vertical drift velocities and east-west electric fields at the magnetic equator. *Journal of Geophysical Research (1896-1977)*, *75*(31), 6249–6259. https://doi.org/10.1029/JA075i031p06249
Woodman, R. F., & Chau, J. L. (2001). Equatorial quasiperiodic echoes from field-aligned irregularities observed over Jicamarca. *Geophysical Research Letters*, *28*(2), 207–209. https://doi.org/10.1029/2000gl000076
Xiong, C., Lühr, H., & Yamazaki, Y. (2019). An opposite response of the low-latitude ionosphere at Asian and American sectors during storm recovery phases: Drivers from below or above. *Journal of Geophysical Research: Space Physics*, *124*, 6266–6280. https://doi.org/10.1029/2019JA026917
Yokoyama, T., & Stolle, C. (2017). Low and midlatitude ionospheric plasma density irregularities and their effects on geomagnetic field. *Space Science Reviews*, *206*, 495–519. https://doi.org/10.1007/s11214-016-0295-7
Zhang, R., Liu, L., Le, H., & Chen, Y. (2017). Equatorial ionospheric electrodynamics during solar flares. *Geophysical Research Letters*, *44*, 4558–4565. https://doi.org/10.1002/2017GL073238
Zhang, R., Liu, L., Le, H., & Chen, Y. (2019). Equatorial ionospheric electrodynamics over Jicamarca during the 6–11 September 2017 space weather event. *Journal of Geophysical Research: Space Physics*, *124*, 1292–1306. https://doi.org/10.1029/2018JA026295